CPW line and realized by LTCC process for smaller size. The size of the miniaturized antenna is about 8×15 mm^2. As a result, we obtained the stop band from 4.8 to 6.3 GHz. The proposed antennas are good candidates for UWB systems where stop band is needed.

REFERENCES

1. Certified Wireless USB. Available at: http://www.usb.org/developers/wusb/
2. S.-W. Su, J.-H. Chou, and K.-L. Wong, "Internal ultrawideband monopole antenna for wireless USB dongle applications", IEEE Trans Antennas Propag 55 (2007), 1180–1183.
3. T. Karacolak and E. Topsakal, "A double-sided rounded bow-tie antenna (DSRBA) for UWB communication", IEEE Antennas Wireless Propag Lett 5 (2006), 446–449.
4. Y.-J. Ren and K. Chang, "An annual ring antenna for UWB communications", IEEE Antennas Wireless Propag Lett 5 (2006), 274–276.
5. M. Sun and Y.P. Zhang, "Miniaturization of planar monopole antennas for ultrawide-band applications", Int Workshop Antenna Technol (2007), 197–200.

A 77-GHz SIX-PORT FMCW COLLISION AVOIDANCE RADAR SENSOR WITH BASEBAND ANALYTICAL CALIBRATION

Bouraima Boukari,[1] **Emilia Moldovan,**[1] **Razvan I. Cojocaru,**[1] **Sofiene Affes,**[1] **Ke Wu,**[2] **Renato G. Bosisio,**[2] **and Serioja Ovidiu Tatu**[1]
[1] Centre Énergie, Matériaux et Télécommunications, Institut national de la recherche scientifique, 800 de la Gauchetière, Montréal, QC H4N 1K6, Canada; Corresponding author: boukari@emt.inrs.ca
[2] Département de Génie Électrical, Poly-Grames Research Center, École Polytechnique de Montréal, Montréal, QC H3T 1J4, Canada

ABSTRACT: *A 77-GHz six-port frequency modulated continuous wave collision avoidance radar sensor is proposed. Velocity and range are determined from the slope of the instantaneous phase of radar beat signals. Digital signal processing techniques are developed to overcome DC offset and amplitude imbalance problems.* © 2009 Wiley Periodicals, Inc. Microwave Opt Technol Lett 51: 720–725, 2009; Published online in Wiley InterScience (www.interscience.wiley.com). DOI 10.1002/mop.24144

1. INTRODUCTION

Frequency modulated continuous wave (FMCW) radars are widely used in collision-avoidance applications because of their simple architecture. In these radars range information appears in the frequency domain and it is obtained by evaluating the frequency of the so called beat signal which is a mixing product of received signal with transmitted one.

Cost efficiency and reliability are main requirements for a commercial application of accurate collision-avoidance radar sensors. Six-port homodyne receivers have been introduced in design of radar sensors to comply with theses requirements [1–5]. In present case, Doppler frequency is read by measuring rate of phase variation of beat signal, and range is measured by phase difference between two properly spaced frequencies. The technique of range determination by measuring the phase difference between discrete frequencies limits the maximum measurable range, so called max-

imum unambiguous range. Major disadvantage of past six-port radar sensors using conventional approach is that six-port must be calibrated [2, 3]. In fact DC offset and amplitude and phase imbalance cause unacceptable measuring errors. Calibration is performed in the frequency domain with network analyzer and important data processing means are necessary in final determination of speed and range [2, 3, 6]. In present paper phase slope measurement is used to replace frequency counting and FFT, as normally used in method of measuring beat frequencies. This single measurement is valid for Doppler frequency and range measurements. Range is determined by an evaluation of phase slope and not by phase measurement itself. This avoids previous stated problem of ambiguous range values. Baseband data processing techniques are also developed to overcome problems related to DC current offset and amplitude imbalance, thereby avoiding need for six-port calibration with network analyzer.

2. SIX-PORT INTERFEROMETER RADAR SENSOR

Six-port technology has been under development over past 30 years for microwave/millimeter-wave measurement applications [6] and [7], and it was for first time used in direct digital receivers [8–10] and radar sensors [1–5]. The six-port circuit is in fact a RF six-port interferometer with a variety of architectures consisting of power dividers, couplers, and phase shifters. These RF components are interconnected in such a way that four different vector sums of reference signal and signal to be directly measured (or down-converted) are produced. Magnitude and phase of unknown signal are determined from amplitudes of four output signals from interferometer.

Figure 1 shows block diagram of six-port circuit for *I/Q* mixer or phase/frequency discriminator used for the radar [3–5] at different operating frequencies. It is a passive circuit composed of
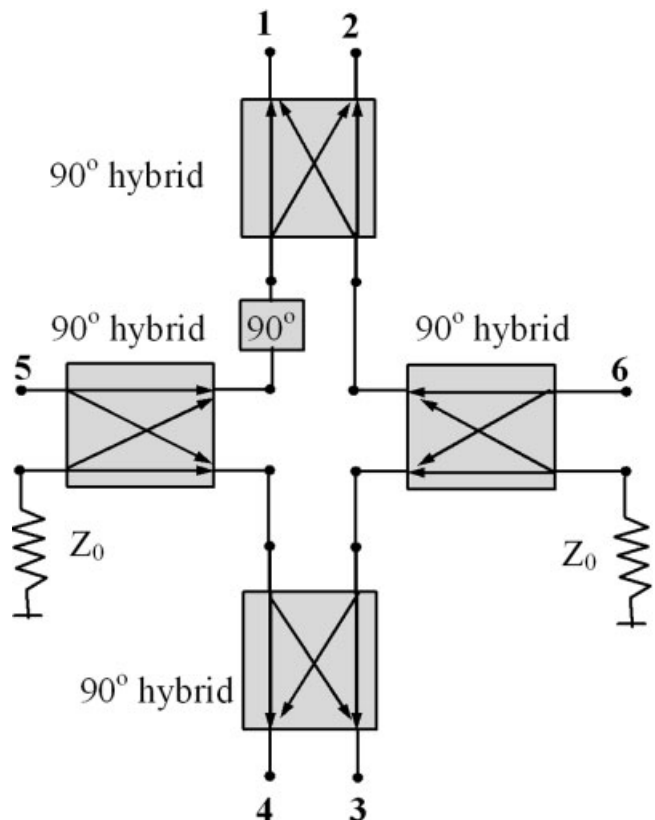

Figure 1 Block diagram of the six-port for the *I/Q* mixer

four 90° hybrid couplers and one 90° phase shifter. A new 77-GHz six-port interferometer has been designed with the following goals:

1. The return losses of designed interferometer six-ports should be very high at center frequency of 77 GHz.
2. Isolation between two input ports and isolation between four output ports must be very high at center frequency. This avoids leakage from local oscillator (LO).
3. Power flow coming from each input port must be equally divided to output ports. In other words the outputs must be well balanced.
4. The phase shift between the generated I and Q signal components must be equal to 90°.

Figure 2 shows the block diagram of radar with six-port interferometer phase/frequency discriminator or I/Q mixer. The millimeter-wave voltage controlled oscillator (VCO) is modulated by a linearly swept frequency signal which gives a linear frequency modulated signal at its output. A portion of the generated FMCW signal is coupled to the six-port mixer at port 5 and serves as reference signal. The main part of generated FMCW signal is amplified and transmitted towards the target. The signal reflected from target is received by radar antenna and amplified using a low noise amplifier (LNA). The four outputs of I/Q mixer are amplified and then A/D converted. A digital signal processor (DSP) is used to calculate relative speed and range of target.

3. RANGE AND SPEED

A new method for determining target range and relative target speed is proposed. The method avoids conventional six-port interferometer calibration for accurate range and speed measurement. In addition DC offset problems are eliminated and amplitude imbalance is improved with baseband signal processing.

The complex beat signal [5] in (see Fig. 2), at DSP input is:

$$\bar{S} = S_I + jS_Q. \tag{1}$$

By taking into account the DC offset and amplitude imbalance, I/Q signals can be written as follows:

$$S_I = A_{0I} + A_I\cos(2\pi f_b t + \varphi_0) = A_{0I} + A_I\cos\varphi, \tag{2}$$

$$S_Q = A_{0Q} + A_Q\cos(2\pi f_b t + \varphi_0) = A_{0Q} + A_Q\sin\varphi. \tag{3}$$
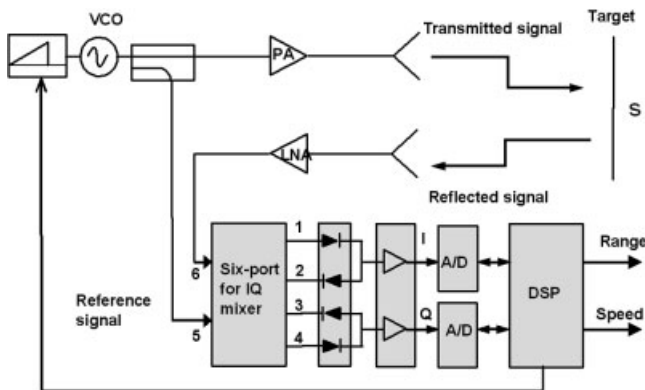

Figure 2 Block diagram of the six-port FMCW radar sensor

In previous equations, A_{0I}/A_{0Q} are DC components, and A_I/A_Q are amplitudes of sinusoidal parts of I and Q signals, respectively.

In the case of amplitude imbalance, the magnitudes of quadrature signals are not equal, i.e., $A_I \neq A_Q$.

S_I and S_Q signals are known, and DC offsets, A_{0I} and A_{0Q}, can be obtained by evaluating their mean values:

$$A_{0I} = \frac{1}{T}\int^{+T} S_I dt, \tag{4}$$

$$A_{0Q} = \frac{1}{T}\int^{+T} S_Q dt. \tag{5}$$

The DC offsets are eliminated by subtraction from S_I and S_Q signals.

To solve amplitude imbalance we need to have both in-phase and quadrature components amplitudes equal. Therefore, we must determine A_I and A_Q and normalize each component. The two amplitudes are calculated from the root mean square values as follows:

$$A_I = \sqrt{2}\sqrt{\frac{1}{T}\int^{+T} (S_I - A_{I0})^2 dt}, \tag{6}$$

$$A_Q = \sqrt{2}\sqrt{\frac{1}{T}\int^{+T} (S_Q - A_{Q0})^2 dt}. \tag{7}$$

The period T must be a multiple of beat signal periods. Since the periods are not known, T is fixed so that it covers several cycles to minimize errors. Now that all the coefficients in (2) and (3) are calculated, the new signal components and the instantaneous phase are found to be:

$$S_I' = \frac{S_I - A_{0I}}{A_I}, \tag{8}$$

$$S_Q' = \frac{S_Q - A_{0Q}}{A_Q}, \tag{9}$$

$$\varphi = 2\pi f_b t + \varphi_0 = \text{Arc tan}\left(\frac{\frac{S_Q - A_{0Q}}{A_Q}}{\frac{S_I - A_{0I}}{A_I}}\right). \tag{10}$$

From (10) the beat frequency can be determined as follows:

$$f_b = \frac{1}{2\pi}\frac{d\varphi}{dt}. \tag{11}$$

Figure 3 shows the waveform of the FMCW signal. The top part of this figure shows plots of frequency versus time for signal transmitted by radar (solid line), and return signal from target received by radar (dotted line). The bottom part of figure shows frequency of output signal generated by radar mixer with transmitted and received input signal frequencies.

The frequency shift due to the range of target moving away from the radar is [11]:
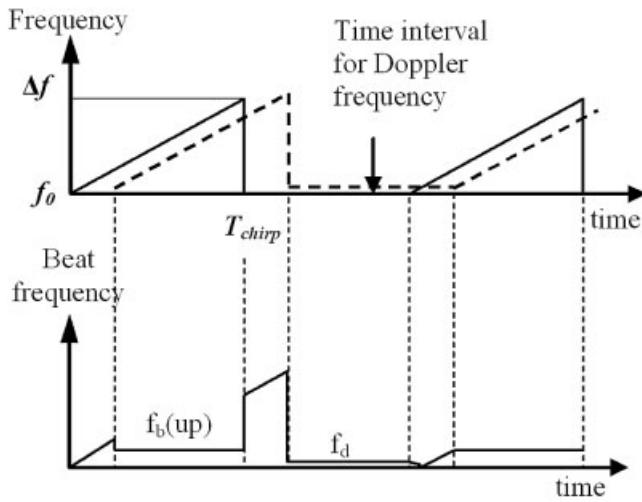
$$f_R = f_b(\text{up}) - f_d. \tag{12}$$

Figure 3 FMCW waveforms

f_b (up) and f_d are, respectively, the beat frequency at rising chirp and the Doppler frequency. It is to be noted that range can be calculated using f_R as follows [11]:

$$R = \frac{cf_R}{2f_{chirp}\Delta f} \qquad (13)$$

From f_d one can find the relative speed [11]:

$$\nu_r = \frac{cf_d}{2f_0} \qquad (14)$$

where c is the speed of light in vacuum, f_0 is the center frequency, Δf is the bandwidth of the FMCW signal, and $F_{chirp} = 1/T_{chirp}$ is the chirp cycle.

4. SIMULATION RESULTS

Design and simulation consist of three sections as follows:

1. The design and electromagnetic simulation of the six-port,
2. Large-signal harmonic balance simulation of the six-port interferometer *I/Q* mixer, and
3. Envelope simulation of entire radar system.

The six-port interferometer circuit was simulated with electromagnetic simulation tool software of Agilent Technologies: momentum of advanced design system (ADS).

The circuit was designed for MHMIC technology on a 127 μm substrate with a relative permittivity of 9.9.

Figure 4 shows the layout of the six-port interferometer circuit. The size of the circuit is 10 mm by 10 mm. The scattering parameters simulation results are shown in Figures 5–7. Figure 5 shows return losses of output ports.

Figure 6, shows isolation between input ports and their return losses.

It is seen that all return losses and isolation are better than 20 dB in 6 GHz bandwidth centered at 77 GHz.

Figure 7 shows a typical transmission from port 5 (input port) to output ports. In this case the amplitude imbalance is better than 0.5 dB over a wide bandwidth (74–80 GHz).
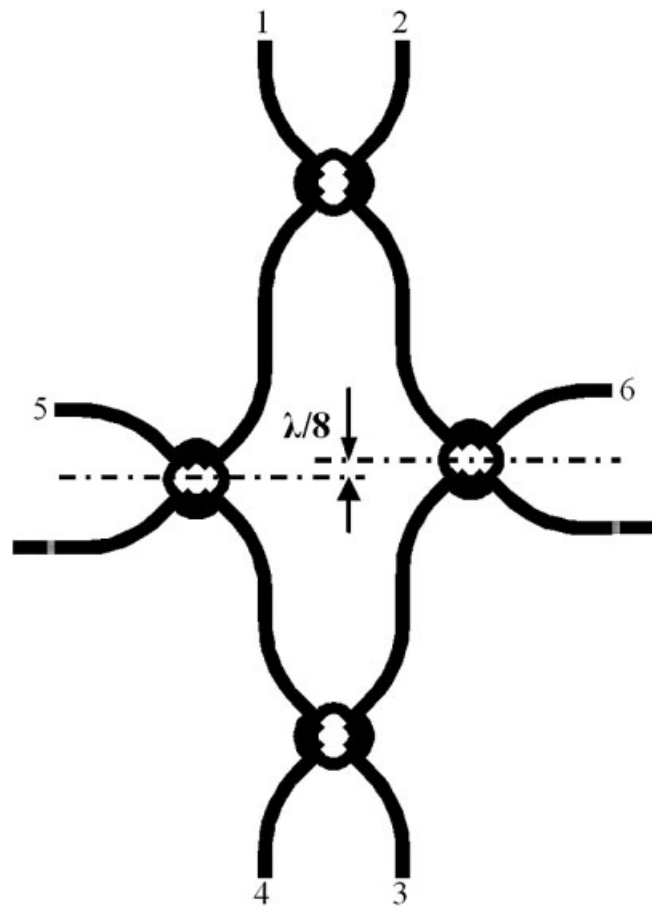
Figure 4 Layout of the six-port junction

To perform advanced system simulations, *S* parameters of six-port model were saved in a data file. This data file was then used as data input to large-signal harmonic balance simulation of mixer along with Spice model of microwave device technology (MDT) flip-chip Schottky diodes.

Figure 8 shows the block schematic of the six-port *I/Q* mixer. To provide a ground return at the IF frequencies, four $\lambda/4$ short-circuit stubs were used. As known, these stubs are open circuits for RF and LO signal. One $\lambda/4$ open-circuit stub is connected to each mixer output preventing LO and RF leakage in IF path. In addition, matching networks (MN) are inserted at the inputs of all Schottky diodes.
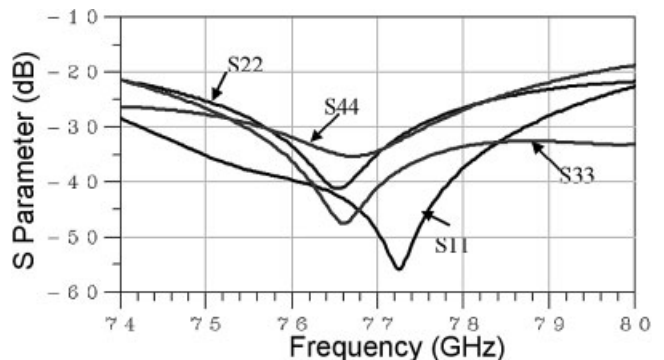

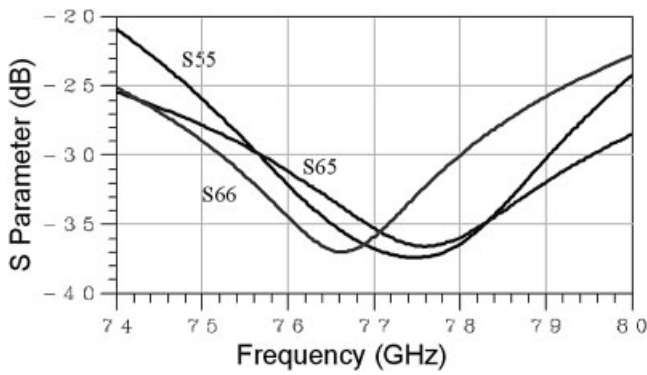**Figure 5** Return losses at the six-port junction output ports

Figure 6 Return losses and isolation at the input ports of the six-port junction

Figure 9 shows the conversion losses of *I* and *Q* signal components versus LO power obtained from simulations. To improve conversion losses, the LO power must be increased. Conversion losses were found to be less than 5 dB when LO signal was 10 dBm. For comparison, the 5 dB conversion loss is less than experimental conversion loss of 13.5 dB of TriQuint semiconductor MMIC downconverting *I/Q* mixer (TGC4702-FC). This improved simulated conversion loss is basically because of the matching networks inserted at the input of each diode.

The entire radar system was simulated on envelope simulator of ADS according to block diagram of FMCW radar system shown in Figure 2. ADS system models of VCO, amplifiers, and filters were used. In addition, models were used for various path lengths taking into account: signal attenuation (radar equation [11]), propagation delay (between radar and target), and Doppler effect. The radar cross-section of target was set to 1 m^2. The simulated radar parameters were as follows:

$$\Delta f = 200.0 \text{ MHz},$$

$$f_0 = 77.0 \text{ GHz},$$

$$f_{chirp} = 1/T_{chirp} = 83.333 \text{ kHz}.$$

In addition: transmitter and receiver antenna gains were 20 dBi each, VCO power was 10 dBm, PA gain was set at 10 dB, and directional couplers were −10dB.

To see improvement with data processing, the complex beat signal was plotted in a polar coordinates system. In the ideal case (no DC
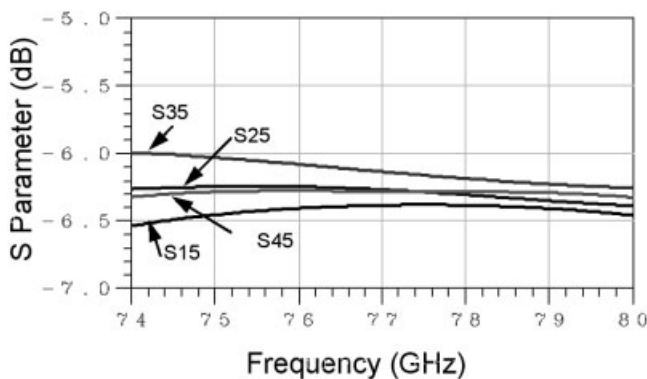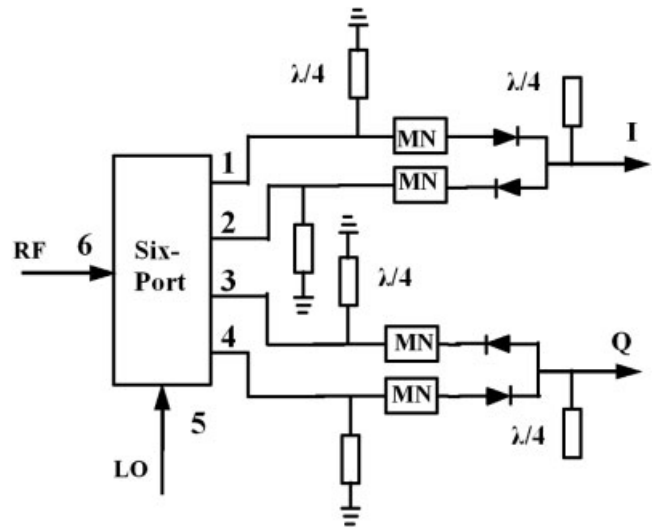

Figure 8 Block schematic of the six-port mixer

offset and circuit structure is well balanced), a circle centered at the coordinates system origin is obtained.

Figures 10 and 11 show the complex beat signals in polar form for a relative target speed of 15 m/s and target range of 20 m, respectively.

Curves (with circle symbols) in theses figures represent the normalized complex unprocessed beat signals.

Curves (in solid line without symbols), are complex processed beat signals for speed and range, respectively. As seen, unprocessed beat signals for speed and range are far from the ideal case. Therefore, determination of phase and beat frequency from these signals will generate unacceptable errors. Curves for processed complex beat signals for speed and range describe quasi-circles centered at origin of polar coordinate system. This shows that ideal case is approached. Other simulations were performed for various ranges and speed values. Tables 1 and 2 summarize these results. The beat frequencies are calculated from *N* = 50 phase points and averaged. The maximum relative error obtained for speed according to Table 1 is 0.025% and maximum relative error for range, according to Table 2 is 1.7%. The improved performance for speed determination is due to fact that a time interval at which no modulation is performed is dedicated to speed measurement. For same sampling frequency, speed resolution is better than that of
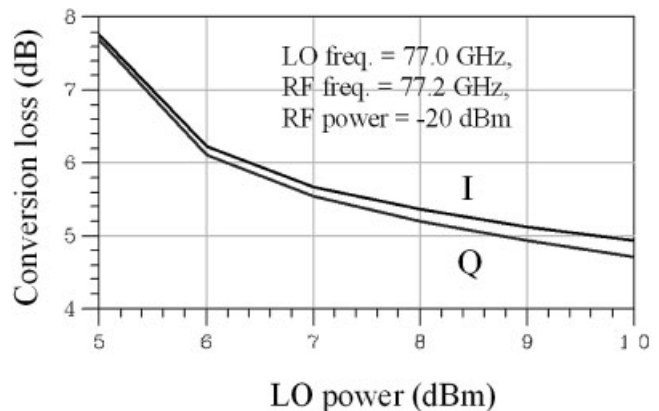

Figure 7 Transmissions from LO port to the output ports of the six-port junction

Figure 9 Conversion loss of the *I* and *Q* signals of the mixer versus LO power
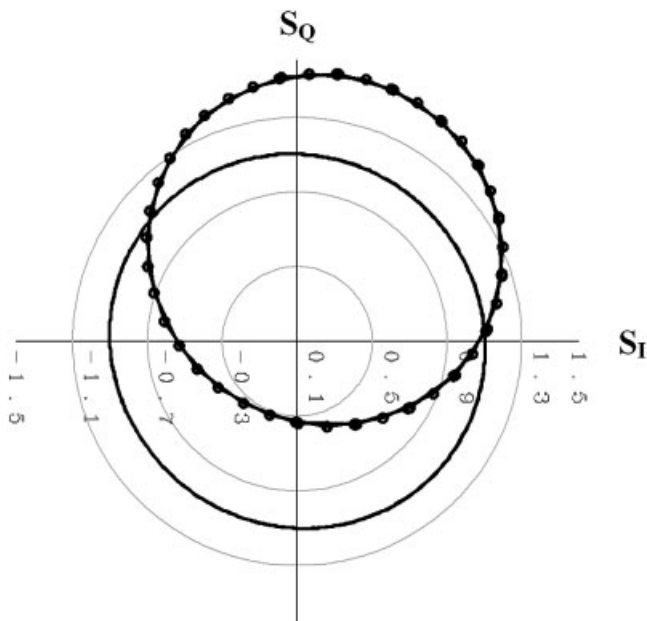
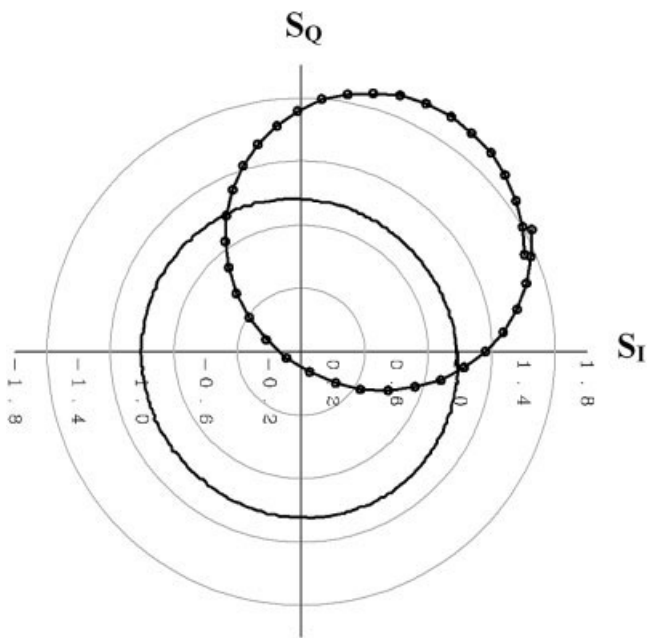**Figure 10** Complex beat signal for the speed of 15 m/s

Figure 11 Complex beat signal for the range of 20 m

TABLE 1 Simulation Results for the Relative Speed (Range = 10 m)

Target Speed (m/s)	Number of Points	Measured Speed (m/s)	Relative Error (%)
10	50	10.00	0.0
20	50	20.00	0.0
30	50	30.00	0.0
40	50	39.99	0.025
50	50	50.01	0.02

TABLE 2 Simulation Results for the Range (Speed = 15 m/s)

Target Range (m)	Number of Points	Measured Range (m)	Relative Error (%)
10	50	10.17	1.7
15	50	15.14	0.93
20	50	20.15	0.77
25	50	25.24	0.96
30	50	30.19	0.63
40	50	40.42	1.05

range because Doppler frequencies are much lower than beat frequencies.

To do a statistical evaluation of range and speed obtained by simulations, a range resolution equal to about half of the 77-GHz wavelength and a speed resolution equal to half of the 77-GHz wavelength per second were chosen. Up to 50 simulations for each range and speed value were performed.

Figures 12 and 13 show histograms for ranges of 25 m and 45 m. Figure 14 shows histogram for speed of 20 m/s. Above histograms show that dispersion of range values is more pronounced than dispersion of speed values.

Standard deviations (SD) were found for following parameters: range of 25 m, SD is 0.07 m or 0.28%; range of 45 m, SD is 0.283 m or 0.6%; speed of 20 m/s, SD is 0.003 m/s or 0.015%.

In comparison, standard deviations of 2.8% and 1.8% were obtained, respectively, for range values of 25 m and 45 m in reference [4]. Present results show that method of determining range by evaluating the slope of the instantaneous phase of beat signal is very good for baseband signal in FMCW six-port radar.
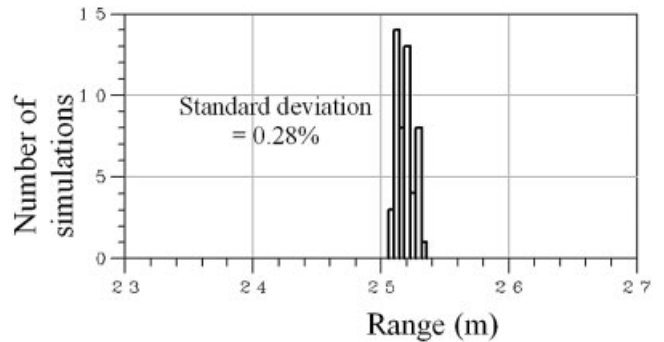

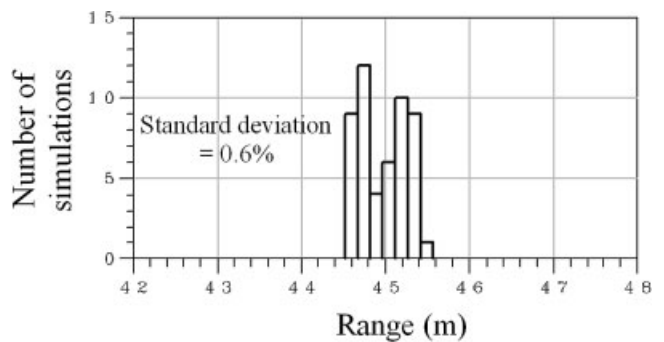**Figure 12** Histogram of the range obtained by simulations for a target situated at 25 m from the radar

Figure 13 Histogram of the range obtained by simulations for a target situated at 45 m from the radar
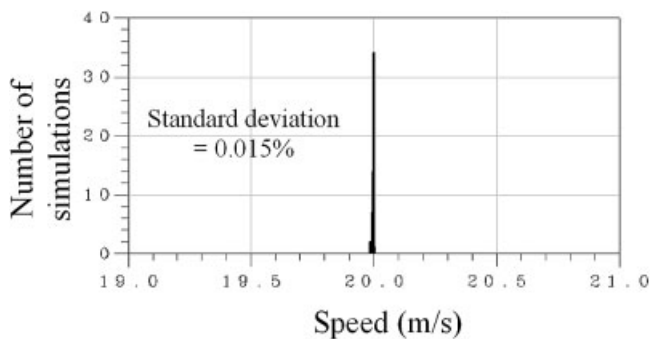
Figure 14 Histogram of the speed obtained by simulations for a target speed of 20 m/s

In fact proposed method is more accurate than past methods of determining range from phase difference between two millimeter-wave signals properly spaced in frequency.

5. CONCLUSIONS

A 77-GHz six-port interferometer for FMCW collision-avoidance radar is presented. Range and speed are determined by evaluating the slope of instantaneous phase of beat signal. Simulation results provide comparison of present range dispersion with those obtained in literature. Range measurements derived from slope of instantaneous phase of baseband beat signal is found to be more accurate than method of determining range from phase difference between two millimeter-wave signals properly spaced in frequency. Proposed method of correcting DC offset and amplitude imbalance for six-port interferometer FMCW with phase/frequency discriminator avoids use of complicated calibration method using network analyzer.

REFERENCES

1. J. Li, K. Wu, and R.G. Bosisio, A collision avoidance radar using six-port phase/frequency discriminator, IEEE MTT-S Int Microw Symp, San Diego, CA (1994), 1553–1556.
2. A. Stelzer, C.G. Diskus, K. Luebke, and H.W. Thim, A microwave position sensor with submillimeter accuracy, IEEE Trans Microw Theor Tech 47 (1999), 2621–2624.
3. G.C. Miguélez, B. Huyart, E. Bergeault, and P.L. Jallet, A new automobile radar based on the six-port phase/frequency discriminator, IEEE Trans Veh Tech 49 (2000), 1416–1423.
4. E. Moldovan, S.O. Tatu, T. Gaman, K. Wu, and R.G. Bosisio, A new 94 GHz six port collision avoidance radar sensor, IEEE Trans Microw Theor Tech 52 (2004), 751-759.
5. B. Boukari, E. Moldovan, S. Affes, K. Wu, R.G. Bosisio, and S.O. Tatu, Six-port FMCW radar sensor configurations, 21st Canadian conference on electrical and computer engineering CCECE2008, Niagara Falls, 2008, pp. 305–308.
6. G.F. Engen, Calibrating the six-port reflectometer by means of sliding terminals, IEEE Trans Microw Theor Tech 26 (1978), 951–957.
7. G.F. Engen, The six-port reflectometer: An alternative network analyzer, IEEE Trans Microw Theor Tech 25 (1977), 1075–1080.
8. J. Li, R.G. Bosisio and K. Wu, Computer and measurement simulation of a new digital receiver operating directly at millimeter-wave frequencies, IEEE Trans Microw Theor Tech 43 (1995), 2766–2772.
9. S.O. Tatu, E. Moldovan, K. Wu, and R.G. Bosisio, A new direct millimeter-wave six-port receiver, IEEE Trans Microw Theor Tech 49 (2001), 2517–2522.
10. S.O. Tatu, E. Moldovan, K. Wu, R.G. Bosisio, and T.A. Denidni, Ka-Band analog front-end for software-defined direct conversion receiver, IEEE Trans Microw Theor Tech 53 (2005), 2768–2776.
11. K. Chang, RF and microwave wireless systems, Wiley, New York, NY, 2000.

CHARACTERIZATION OF THE POLARIZATION IN THE SPUN FIBERS

L. Cherbi, A. Azrar, M. Mehenni, and R. Aksas
Department of Electrical and Electronic Engineering, National Polytechnic School, 10 Avenue Hassan Badi, BP 182 El-Harrach, Algiers 16200, Algeria; Corresponding author: take_azrar_2007@yahoo.com

ABSTRACT: *The polarization mode dispersion (PMD) is a difficult phenomenon to compensate in the optical fiber. Its reduction can be achieved by the spinning process that provokes the rotation of the birefringence axes of the fiber inciting a coupling of its modes that is controlled at the time of its manufacture. In this work, the Jones Matrix Eigen-Analysis method (JME) is used to characterize the spun fibers to evaluate their PMD and to prove that it is distinctly lower than the standards fibers PMD. Furthermore, the differential group delays (DGD) of spun fibers is determined using the photon counting optical time-domain reflectometry (C-OTDR) method. The obtained results are compared with those found in the JME method. It is noted that the two methods yield practically identical values. The determination of the beat length and the spin period of spun fibers is carried out using the polarization-sensitive optical frequency-domain reflectometer (POFDR). © 2009 Wiley Periodicals, Inc. Microwave Opt Technol Lett 51: 725–731, 2009; Published online in Wiley InterScience (www.interscience.wiley.com). DOI 10.1002/mop.24143*

1. INTRODUCTION

The typical tolerance of a transmission system using the optical fiber to the polarization mode dispersion (PMD) is equal approximately to 10% of the period bit. This results in 40 ps in the 2.5 Gb/s system, 10 ps in the 10 Gb/s system, and only 2.5 ps in the 40 Gbs/s system [1]. As the debit should increase, the requirement for the PMD becomes stricter. It is therefore important to use the fibers with low PMD in the communication systems. In the past decade, some considerable efforts have been made to understand the origin of the PMD and to attenuate its effect in the transmission systems. There are two ways to reduce the PMD in an optical fiber. In the first, the asymmetries in the profile of the refractive index and the stress are minimized [2]. It implies improvements in the industrial process of the fiber manufacture to assure a better geometry and thus reduce the rate of its stress. The second introduces the coupling of the polarization modes, which is controlled while spinning the fiber during its manufacture [3]. The spinning has been used in the fiber manufacturing since the beginning of the 1990 years, and it showed that it was an efficient technique to reduce the PMD in the fiber.

In this work, the PMD in the spun fibers is measured by applying the JME method to verify its reduction compared to the one of the classical fibers. In addition, the COTDR, POFDR high-resolution methods of reflectometry are used to calculate and to measure the polarization characteristics of spun fibers such as